Oxygen-Atom Transfer Reactivity of Axially Ligated Mn(V)−Oxo Complexes: Evidence for Enhanced Electrophilic and Nucleophilic Pathways

Heather M. Neu,[†] Tzuhsiung Yang,[†] Regina A. Baglia,[†] Timothy H. Yosca,[§] Michael T. Green,*,[§] Matthew G. Quesne,[‡] Sam P. de Visser,*,[‡] and David P. Goldberg*,[†]

[†]Department of Chemistry, The Johns Hopkins University, Baltimore, Maryland 21218, United States

[§]Department of Chemistry, Pennsylvania State University, University Park, Pennsylvania 16802, United States

[‡]The Manchester Institute of Biotechnology and School of Chemical Engineering and Analytical Science, The University of Manchester, 131 Princess Street, Manchester M1 7DN, United Kingdom

S *Supporting Information*

ABSTRACT: Addition of anionic donors to the manganese(V)−oxo corrolazine complex $Mn^V(O)(TBP_8Cz)$ has a dramatic influence on oxygen-atom transfer (OAT) reactivity with thioether substrates. The six-coordinate anionic $[Mn^V(O)(TBP_8Cz)(X)]^-$ complexes ($X = F^-$, N_3^-, OCN^-) exhibit a ~5 cm^{-1} downshift of the Mn−O vibrational mode relative to the parent $Mn^V(O)(TBP_8Cz)$ complex as seen by resonance Raman spectroscopy. Product analysis shows that the oxidation of thioether substrates gives sulfoxide product, consistent with single OAT. A wide range of OAT reactivity is seen for the different axial ligands, with the following trend determined from a comparison of their second-order rate constants for sulfoxidation: five-coordinate ≈ thiocyanate ≈ nitrate < cyanate < azide < fluoride ≪ cyanide. This trend correlates with DFT calculations on the binding of the axial donors to the parent $Mn^V(O)(TBP_8Cz)$ complex. A Hammett study was performed with $p\text{-}X\text{-}C_6H_4SCH_3$ derivatives and $[Mn^V(O)(TBP_8Cz)(X)]^-$ ($X = CN^-$ or F^-) as the oxidant, and unusual "V-shaped" Hammett plots were obtained. These results are rationalized based upon a change in mechanism that hinges on the ability of the $[Mn^V(O)(TBP_8Cz)(X)]^-$ complexes to function as either an electrophilic or weak nucleophilic oxidant depending upon the nature of the *para*-X substituents. For comparison, the one-electron-oxidized cationic $Mn^V(O)(TBP_8Cz^{•+})$ complex yielded a linear Hammett relationship for all substrates ($\rho = -1.40$), consistent with a straightforward electrophilic mechanism. This study provides new, fundamental insights regarding the influence of axial donors on high-valent $Mn^V(O)$ porphyrinoid complexes.
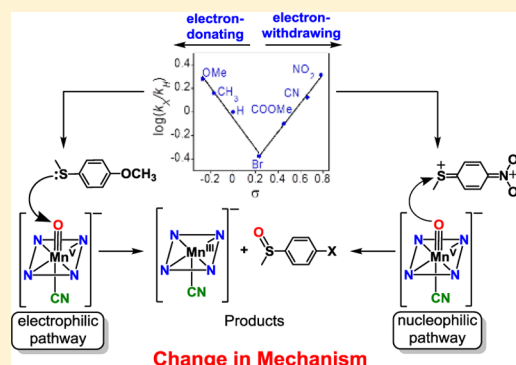
INTRODUCTION

A key structural factor that contributes to metal-oxo reactivity in heme enzymes is the nature of the axial ligands coordinated trans to the oxo group. The concept of axial ligand tuning is exemplified in the powerful oxygenating enzyme Cytochrome P450, in which the anionic, deprotonated Cys ligand is believed to play a critical role. It has been suggested that the Cys in Cyt-P450 plays an essential role in modulating the reactivity of Compound-I (Cpd-I), $Fe^{IV}(O)(porph^{•+})(Cys)$, (porph = porphyrin) which is the key intermediate prior to substrate oxidation.[1−7] Further evidence for the importance of the axial donor lies in the fact that it is the major feature that distinguishes broad classes of heme enzymes, with Cyt-P450 and chloroperoxidase (CPO) containing an axial Cys, peroxidase containing an axial His,[8−10] and catalase containing an axial Tyr ligand.[11,12]

The preparation of synthetic analogs of heme enzymes has provided a means to test mechanistic hypotheses regarding the influence of axial donors. Synthetic models of heme active sites are particularly useful for examining complexes that are analogous to the highly unstable intermediates in enzyme systems, including high-valent metal-oxo species. Regarding the influence of axial donors on these species, a potential advantage of model systems is the ability to rationally tune the nature of the axial ligand by varying its structural and electronic properties in a systematic fashion. The influence of axial ligands on high-valent, iron-oxo porphyrin models has been investigated, including the examination of the effects of axial donors on oxygen-atom transfer (OAT) reactivity. For example, axial ligands were shown to enhance the reactivity of $Fe(O)(porph)$ in epoxidations.[13−21] A recent study on the effects of axial ligation on Cpd-I analogs, $Fe^{IV}(O)(porph^{•+})(X)$, provided a detailed thermodynamic analysis which led to a possible explanation for the trend in OAT reactivity versus axial donor.[15] The mechanisms of these reactions and especially the exact role played by the axial ligands are still not well understood.

In contrast to Fe(O) species, the influence of axial donors on analogous Mn(O) porphyrinoid complexes has been much less studied, with very few systematic investigations for a wide range of axial ligands reported to date.[22−30] One of the few examples comes from Chang and co-workers, who showed that the reactivity of an $Mn^V(O)$ corrole toward styrene can be enhanced by 10-fold with an imidazole as an axial ligand.[23] The effects of axial donors on nonheme Mn(O) complexes such as Mn(O)-(salen)(X) have been reported.[31−34] However, direct structural, spectroscopic, or reactivity information on these complexes is in general quite limited because of the transient nature of these species.[31]

Previously, we took advantage of our ability to isolate and definitively characterize a relatively stable high-valent $Mn^V(O)$ complex $Mn^V(O)(TBP_8Cz)$ (TBP_8Cz = octakis(*p-tert*-butylphenyl)corrolazinato$^{3−}$), which contains a ring-contracted porphyrinoid ligand, in order to examine the influence of cyanide and fluoride ions on C−H activation. Indirect evidence was obtained that suggested $CN^−$ and $F^−$ were weakly bound *trans* to the terminal oxo ligand and caused significant increases in H-atom abstraction rates.[35] More recently, we used X-ray absorption spectroscopy to characterize one of these complexes, $[Mn^V(O)(TBP_8Cz)(CN)]^−$, and showed that $CN^−$ was indeed coordinated to the metal while leaving the short Mn−O bond intact.[36] Addition of the $CN^−$ donor caused a large rate enhancement in OAT to thioanisole, giving the predicted two-electron reduced Mn^{III} complex and sulfoxide product.

Herein we describe a comprehensive study regarding the influence of a wide range of anionic axial ligands on the OAT reactivity of an $Mn^V(O)$ porphyrinoid complex. Significant rate enhancements for OAT to thioether substrates are seen for different axial donors. The use of a series of p-X-$C_6H_4SCH_3$ substrates provides a range of OAT rates for the cyanide- and fluoride-ligated $Mn^V(O)$ complexes, revealing unexpected "V-shaped" Hammett plots. These results point to a dramatic switch in mechanism for OAT, depending upon the nature of the substrate. This work provides new, fundamental insights regarding the influence of axial donors on the OAT reactivity of rarely observed $Mn^V(O)$ porphyrinoid complexes.

■ EXPERIMENTAL SECTION

Materials. All reactions were performed under an argon atmosphere using dry solvents and standard Schlenk techniques. The $Mn^{III}(TBP_8Cz)$ and $Mn^V(O)(TBP_8Cz)$ complexes were synthesized according to published methods.[37] Solvents were purified via a Pure-Solv solvent purification system from Innovative Technologies, Inc. $H_2^{18}O$ (97% ^{18}O) was purchased from Cambridge Isotopes, Inc. All other reagents were purchased from Sigma-Aldrich at the highest level of purity and used as received.

Instrumentation. UV−vis spectroscopy was performed on a Hewlett-Packard 8542 diode-array equipped with HP Chemstation software. A filter was placed between the spectrometer light and the sample to prevent bleaching of $[Mn^V(O)(TBP_8Cz)(X)]^−$ from UV light (<400 nm). The temperature-dependent kinetics were performed on a Hewlett-Packard 8453 diode-array spectrophotometer equipped with an Unisoku thermostat cell holder. Gas chromatography (GC) was performed on an Agilent 6850 gas chromatograph fitted with a DB-5 5% phenylmethyl siloxane capillary column (30 m × 0.32 mm × 0.25 μm) and equipped with a flame-ionization detector. GC mass spectrometry (GC-MS) was performed on an Agilent 6850 gas chromatograph fitted with a DB-5 5% phenylmethyl siloxane capillary column and equipped with a mass spectrometer. LDI-TOF was conducted on a Bruker Autoflex III TOF/TOF instrument equipped with a nitrogen laser at 335 nm using an MTP 384 ground steel target plate. ^{31}P NMR spectra were recorded on a Bruker Avance 400 MHz

NMR spectrometer at 298 K. All spectra were taken in 5 mm o.d. NMR tubes, and chemical shifts were reported as δ values from standard peaks.

Resonance Raman Sample Preparation. A solution of $Mn^V(O)$-(TBP_8Cz) (1 mM) in CH_2Cl_2 (250 μL) at 25 °C was combined with $Bu_4N^+X^−$ (X = F, N_3, OCN at 1 M). Samples were loaded into an EPR tube, immediately frozen in liquid nitrogen, and stored at 77 K until measurements were performed.

Resonance Raman Spectroscopy. Resonance Raman spectra were recorded on a triVista 555 triple monochromator (900/900/2400 gr/mm) equipped with a CCD camera (1340 × 100 pixels). A 413.2 nm line of a krypton-ion laser was used for excitation. The laser power was <15 mW at the sample to reduce the risk of photoreduction. 900/900/2400 gr/mm gratings provided a resolution of 0.69 cm$^{−1}$ per CCD pixel at 413.2 nm. Samples were held in an EPR finger-dewar (77 K) in a 135° backscattering arrangement. Raw spectra were analyzed using the program Igor Pro for background subtraction. No smoothing procedures were performed on the raw data.

Product Analysis. In a typical reaction, a stirring solution of $Mn^V(O)(TBP_8Cz)$ (0.2 or 5 mM) in CH_2Cl_2 (3 mL) was combined with an anionic donor $Bu_4N^+F^−$ (1.3 or 12 mM) at 25 °C. To initiate the reaction, dimethyl sulfide (DMS): 11 M or triphenylphosphine (PPh$_3$): 5 mM was added. Isosbestic conversion of $[Mn^V(O)(TBP_8Cz)(F)]^−$ (λ_{max} = 419, 634 nm) to $[Mn^{III}(TBP_8Cz)(F)]^−$ (λ_{max} = 428, 471, 680 nm) was observed by UV−vis spectroscopy. Upon completion of the reaction, the solution was concentrated to ∼50 μL under vacuum. The phosphine reaction was dissolved in $CDCl_3$ and analyzed by ^{31}P NMR. The yield was obtained by comparing the integration of the product peak, triphenylphosphine oxide, to that of the reactant peak (PPh$_3$). To analyze the DMS reaction, *n*-decane was added as an internal standard, and the solution was immediately analyzed by GC-FID. The product, dimethyl sulfoxide (DMSO), was identified by comparison with a standard sample. Yields were obtained by comparing the integration of the product peak with the integration of the internal standard peak. All yields are an average of two runs.

OAT Reaction of $[Mn^V(O)(TBP_8Cz)(X)]^−$ with DMS and Dibutyl Sulfide. In a typical reaction, a solution of $Mn^V(O)(TBP_8Cz)$ (11 μM) in CH_2Cl_2 (2 mL) at 25 °C was combined with $Bu_4N^+X^−$ (11 mM) (X = N_3, OCN, SCN, NO_3) or $Bu_4N^+F^−$·3H_2O (0.03 M). Excess DMS or dibutyl sulfide (DBS) was added to begin the reaction. The changes in absorbance were monitored by UV−vis spectroscopy showing the isosbestic decay of $[Mn^V(O)(TBP_8Cz)(X)]^−$ (λ_{max} = 419, 634 nm) and formation the of $[Mn^{III}(TBP_8Cz)(X)]^−$. A filter was placed between the spectrometer light and the sample to prevent bleaching of $[Mn^V(O)$-$(TBP_8Cz)(X)]^−$ from UV light (<400 nm). The pseudo-first-order rate constants, k_{obs}, were obtained by nonlinear least-squares fitting (eq 1) of the growth in absorbance of $[Mn^{III}(TBP_8Cz)(X)]^−$ at 680−693 nm or decay of $[Mn^V(O)(TBP_8Cz)(X)]^−$ at 634 nm versus time:

$$Abs_t = Abs_f + (Abs_0 − Abs_f)\ exp(−k_{obs}t) \qquad (1)$$

where Abs_f = final absorbance, Abs_0 = initial absorbance, and Abs_t = absorbance at time (t). Second-order rate constants were obtained from the slope of the best-fit line of the linear plot of k_{obs} versus substrate concentration.

Measurement of the Binding Constant for Fluoride to $Mn^V(O)(TBP_8Cz)$. A solution of $Mn^V(O)(TBP_8Cz)$ (10 μM) in CH_2Cl_2 (2 mL) at 25 °C was combined with DBS (2.7 mM). The reaction was initiated by the addition of $Bu_4N^+F^−$·3H_2O (1.7−59 mM). The changes in absorbance were monitored by UV−vis spectroscopy showing the isosbestic decay of $[Mn^V(O)(TBP_8Cz)(F)]^−$ (λ_{max} = 419, 634 nm) and formation of $[Mn^{III}(TBP_8Cz)(F)]^−$ (λ_{max} = 469, 680 nm). The pseudo-first-order rate constants, k_{obs}, were obtained by nonlinear least-squares fitting (eq 1) of the growth in absorbance of $[Mn^{III}(TBP_8Cz)(F)]^−$ at 680 nm versus time. A plot of k_{obs} versus $[F^−]$ showed saturation behavior.

The data were modeled for a 1:1 binding event as shown in eq 2, where the association constant K = $k_1/k_{−1}$, k_2 is the pseudo-first-order rate constant for a given concentration of DMS, and $[F^−]_{total}$ is the total concentration of TBAF.[38] A fit of 1/k_{obs} and 1/$[F^−]_{total}$ plot is given in eq 3.

$$k_{\text{obs}} = k_2 \left(\frac{\text{K}[\text{F}^-]_{\text{total}}}{1 + \text{K}[\text{F}^-]_{\text{total}}} \right) \tag{2}$$

$$\frac{1}{k_{\text{obs}}} = \frac{1 + \text{K}[\text{F}^-]_{\text{total}}}{k_2\text{K}[\text{F}^-]_{\text{total}}} = \frac{1}{k_2\text{K}[\text{F}^-]_{\text{total}}} + \frac{1}{k_2} \tag{3}$$

Linear Free Energy Correlations for OAT of [Mn^V(O)(TBP$_8$Cz)-(X)]$^-$ to *para*-Substituted Thioanisoles. A solution of Mn^V(O)-(TBP$_8$Cz) (12 μM for CN$^-$; 15 μM for F$^-$) in toluene (X = CN$^-$) or CH$_2$Cl$_2$ (X = F$^-$) (2 mL) at 25 °C was combined with a *para*-substituted thioanisole (0.13 M). The reaction was initiated by the addition of Bu$_4$N$^+$X$^-$ (12 mM, X = CN$^-$; 15 mM, X = F$^-$). The changes in absorbance were monitored by UV−vis spectroscopy showing the isosbestic decay of [Mn^V(O)(TBP$_8$Cz)(X)]$^-$ (λ_{max} = 419, 634 nm) and formation of [Mn^{III}(TBP$_8$Cz)(X)]$^-$ (λ_{max} = 443, 492, 694 nm, X = CN$^-$; λ_{max} = 470, 679 nm, X = F$^-$). The pseudo-first-order (k_{obs}) rate constants were obtained as described above. The log(k_X/k_H) for each *para*-substituted thioanisole was graphed versus its Hammett constant (σ).[39]

Linear Free Energy Correlations for OAT of Mn^V(O)(TBP$_8$Cz$^{\bullet+}$) to *para*-Substituted Thioanisoles. Following an earlier report,[40] a solution of Mn^V(O)(TBP$_8$Cz) (11 μM) in CH$_2$Cl$_2$ (2 mL) at 25 °C was combined with a one-electron oxidant [(4-BrC$_6$H$_4$)$_3$N$^{\bullet+}$](SbCl$_6^-$) (11 μM) and monitored by UV−vis spectroscopy which showed the isosbestic conversion of Mn^V(O)(TBP$_8$Cz) (λ_{max} = 419, 634 nm) to [Mn^V(O)(TBP$_8$Cz$^{\bullet+}$)] (λ_{max} = 410, 780 nm). Once complete formation of the Mn^V(O)(TBP$_8$Cz$^{\bullet+}$) complex was observed the OAT reaction was initiated by the addition of a *para*-substituted thioanisole (0.13 M). The changes in absorbance were monitored by UV−vis spectroscopy showing the isosbestic decay of [Mn^V(O)(TBP$_8$Cz$^{\bullet+}$)] (λ_{max} = 410, 780 nm) and formation of [Mn^{IV}(TBP$_8$Cz)]$^+$ (λ_{max} = 433, 669, and 722 nm). The pseudo-first-order (k_{obs}) rate constants were obtained by nonlinear least-squares fitting (eq 1) of the growth in absorbance of [Mn^{IV}(TBP$_8$Cz)]$^+$ at 722 nm versus time. The log(k_X/k_H) for each *para*-substituted thioanisole was graphed versus its Hammett constant (σ).[39]

■ RESULTS AND DISCUSSION

OAT Reactivity of [Mn^V(O)(TBP$_8$Cz)(F)]$^-$ with Thioether and Phosphine Substrates. Kinetic analysis showed that the oxidation of thioether substrates by Mn^V(O)(TBP$_8$Cz) was relatively slow, with second-order rate constants of 2.0 × 10^{-3} M^{-1} s^{-1} for DMS and 3.8 × 10^{-4} M^{-1} s^{-1} for DBS.[40] The addition of CN$^-$ to Mn^V(O)(TBP$_8$Cz) dramatically increased the rates of sulfoxidation, giving a second-order rate constant of 9.2 M^{-1} s^{-1} for DBS.[36] We next sought to extend our study on the influence of anionic donors and determine whether a correlation with reactivity and the nature of the axial donor could be made. Investigations were initiated by examining the reactivity of the fluoride anion. Addition of Bu$_4$N$^+$F$^-$ (TBAF) to Mn^V(O)-(TBP$_8$Cz) in the presence of excess DMS as substrate was monitored in CH$_2$Cl$_2$ at 25 °C (Scheme 1). The UV−vis spectra are shown in Figure 1a and reveal isosbestic conversion of the Mn^V-oxo complex to the axially ligated complex [Mn^{III}(TBP$_8$Cz)(F)]$^-$, with a split Soret band at 428 and 471 nm. As previously observed, there is little change in the UV−vis spectrum for Mn^V(O)(TBP$_8$Cz) upon addition of F$^-$, but splitting in the Soret region of the corresponding [Mn^{III}(TBP$_8$Cz)(F)]$^-$ complex is clearly seen in Figure 1b.[35,36] A related complex (Et$_4$N)[Mn^{III}(TBP$_8$Cz)(Cl)] was crystallographically characterized and exhibited a similar splitting in the Soret band.[37,41] With the addition of excess TBAF, the OAT reaction was complete in 1.5 h, and analysis by GC-FID revealed DMSO as the major oxidation product (85%). In comparison, the oxidation of DMS by the five-coordinate Mn^V(O)(TBP$_8$Cz) is much slower, taking over 17 h for completion.

Scheme 1. Oxidation of Thioether and Phosphine Substrates by [Mn^V(O)(TBP$_8$Cz)(F)]$^-$
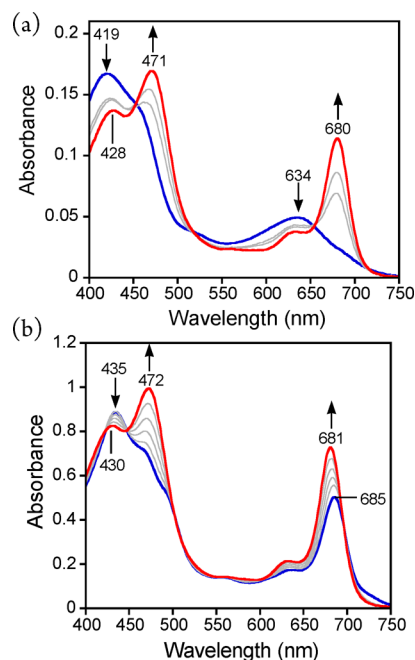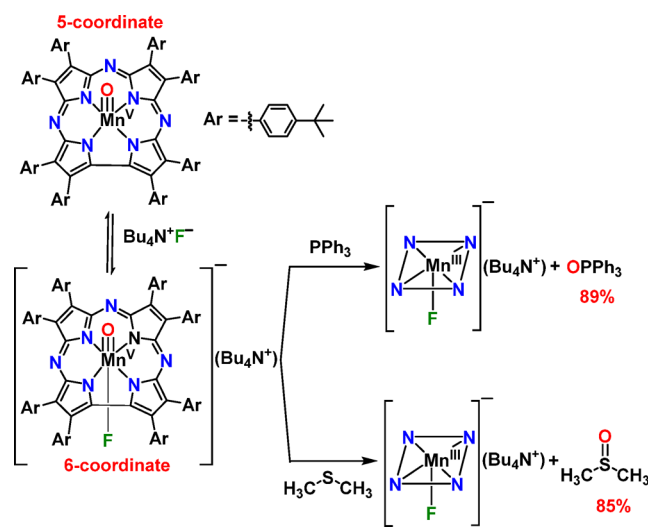
Figure 1. (a) UV−vis spectral changes (0−1.5 h) for the reaction of Mn^V(O)(TBP$_8$Cz) + Bu$_4$N$^+$F$^-$ (6 equiv) (419, 634 nm) with excess DMS to give [Mn^{III}(TBP$_8$Cz)(F)]$^-$ (428, 471, 680 nm) in CH$_2$Cl$_2$ at 25 °C. (b) UV−vis spectral titration of Mn^{III}(TBP$_8$Cz) (435, 685 nm) (blue line) with Bu$_4$N$^+$F$^-$ (0−1 equiv) to give [Mn^{III}(TBP$_8$Cz)(F)]$^-$ (430, 472, 681 nm) in CH$_2$Cl$_2$ at 25 °C.

An alternate O-atom acceptor, PPh$_3$, showed similar reactivity, resulting in the rapid conversion of [Mn^V(O)(TBP$_8$Cz)(F)]$^-$ to [Mn^{III}(TBP$_8$Cz)(F)]$^-$. The ^{31}P NMR spectrum (Figure S1) of the reaction mixture identified OPPh$_3$ as the major product in 89% yield (Scheme 1). Thus, the Mn^V(O) complex, in the presence of TBAF, reacts rapidly and quantitatively with both thioether and phosphine O-atom acceptors to give sulfoxide or phosphine oxide products via a formal OAT process.

Dependence of OAT Rates on Fluoride Concentration. In earlier work we showed that the rates of H-atom abstraction by Mn^V(O)(TBP$_8$Cz) with C−H substrates depended on the concentration of added TBAF.[35] A plot of pseudo-first-order rate

constants (k_{obs}) versus [TBAF] for two different C–H substrates gave a saturation curve that was successfully modeled as a 1:1 binding equilibrium.[35] In the present study, the rates of sulfoxidation of DBS under pseudo-first-order conditions were similarly monitored by UV–vis, and the concentration of TBAF was varied. Plots of the absorbance associated with the decay and growth of the Mn^V and Mn^{III} complexes, respectively, were well-fit to a single exponential kinetic model (Figure S2). The resulting k_{obs} values were plotted versus $[F^-]$ (Figure 2a) and
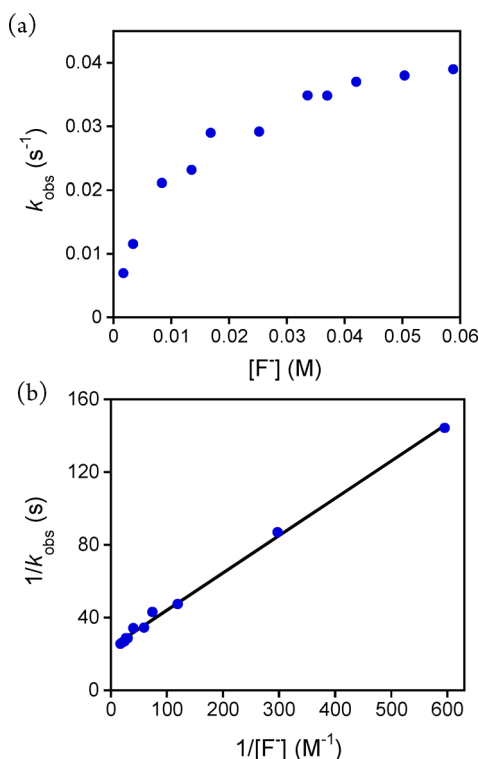
Figure 2. (a) Dependence of the k_{obs} values on the concentration of $Bu_4N^+F^-$ for the reaction of $Mn^V(O)(TBP_8Cz)$ + DBS (270 equiv) in CH_2Cl_2 at 25 °C. (b) Double-reciprocal plot of $1/k_{obs}$ versus $1/[F^-]$ (blue circles) and best fit line (black).

exhibit saturation behavior, indicative of a rapid pre-equilibrium for the binding of F^- prior to the rate-determining step. A double reciprocal plot ($1/k_{obs}$ versus $1/[F^-]_{total}$) (Figure 2b) reveals good linearity, with a best fit that gives a binding constant of $K(F^-) = 115 \pm 4\ M^{-1}$. This value is in good agreement with the binding constants found previously for fluoride anion and the $Mn^V(O)$ complex in reactions with C–H substrates (163 ± 7 and $191 \pm 10\ M^{-1}$).[35] These results provide strong evidence that addition of excess F^- leads to the formation of a six-coordinate $Mn^V(O)$ complex with the fluoride ligated relatively weakly *trans* to the oxo group.

Resonance Raman Spectroscopy of the Six-coordinate $Mn^V(O)$ Complexes. The binding of X^- to $Mn^V(O)(TBP_8Cz)$ can be described according to the simple equilibrium in eq 4:

$$Mn^V(O)(TBP_8Cz) + X^- \rightleftharpoons [Mn^V(O)(TBP_8Cz)(X)]^-$$
$$\text{five-coordinate} \qquad\qquad \text{six-coordinate}$$

(4)
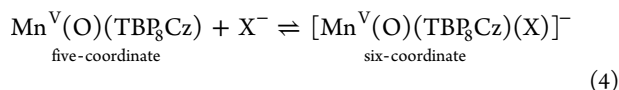
The six-coordinate complexes were examined by resonance Raman spectroscopy for X = F^-, N_3^-, and OCN^-. Excess X^- was added to push the equilibrium in eq 4 to favor the six-coordinate complexes in CH_2Cl_2. Frozen solution samples were excited with

the 413.2 nm krypton-ion excitation line at 77 K. A Mn–O vibrational mode for the five-coordinate $Mn^V(O)(TBP_8Cz)$ starting complex was identified at 981 cm^{-1}, which downshifts to 939 cm^{-1} upon ^{18}O substitution (Figure S3). This 42 cm^{-1} shift is in good agreement with diatomic harmonic oscillator predictions as well as previously published results.[42] The spectra for the F^-, N_3^-, and OCN^- complexes are shown in Figure 3,
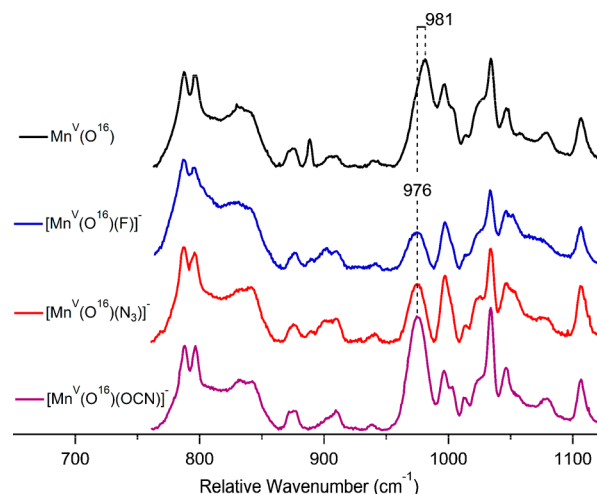
Figure 3. Low-frequency resonance Raman spectra of $^{16}O\ [Mn^V(O)-(TBP_8Cz)(X)]^-$ where X = no ligand, F^-, N_3^-, or OCN^-. The resonances near 900 cm^{-1} were used to scale the spectra. Data were collected using a 413.2 nm krypton-ion laser line.

together with the five-coordinate starting material. The Mn–O mode clearly downshifts by 5 cm^{-1} to 976 cm^{-1} relative to the starting complex. The identity of the peak at 976 cm^{-1} was verified using ^{18}O labeling for the F^- and N_3^- complexes (Figures S4 and S5). These results provide strong evidence that the anionic donors are coordinated *trans* to the terminal oxo ligand, thereby inducing a subtle weakening of the Mn–O vibrational mode. Similar effects on the metal-oxo stretch were seen upon variation of *trans* axial donors in both heme and nonheme $Fe^{IV}(O)$ complexes.[15,43,44]

Kinetic Studies of OAT for a Series of Anionic Axial Donors. A broad series of anionic axial ligands (X^-), in conjunction with two thioether substrates (DMS and DBS), were employed for kinetic studies (Scheme 2). An example of the

Scheme 2. Kinetic Model for OAT to Thioether Substrates

R = -CH$_3$ or -(CH$_2$)$_3$CH$_3$
X = CN, F, N$_3$, OCN, NO$_3$, SCN
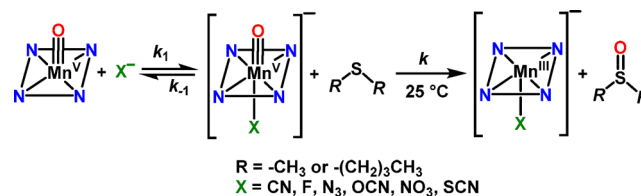
UV–vis spectral changes observed for these OAT reactions is shown in Figure 4, where X = N_3^-. Good isosbestic behavior is seen, and the final spectrum matches that for $[Mn^{III}(TBP_8Cz)-(N_3)]^-$. Plots of absorbance versus time for the decay of the $Mn^V(O)$ complex (634 nm) and the appearance of the $Mn^{III}(N_3^-)$ complex (685 nm) are shown in the inset, Figure 4. These plots, along with the plots for the other axial donors, were well fit by a single exponential model, consistent with the
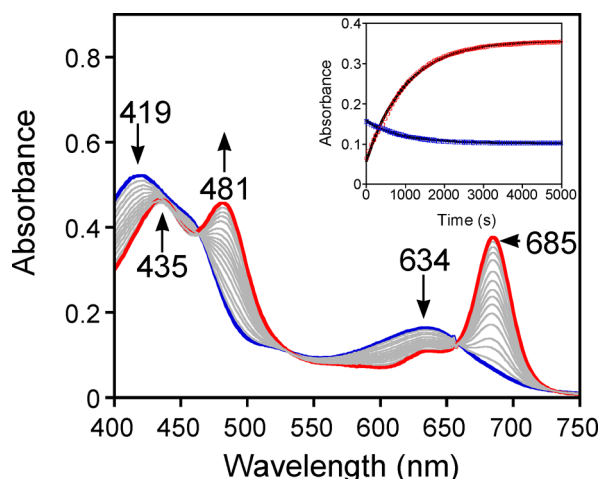
Figure 4. UV−vis spectral changes for the reaction of $[Mn^V(O)(TBP_8Cz)(N_3)]^-$ (9 μM) (419, 634 nm) with DMS (4.0 mM) in CH_2Cl_2 at 25 °C. Inset: changes in absorbance versus time for the growth of $[Mn^{III}(TBP_8Cz)(N_3)]^-$ (685 nm) (open red circle) and the decay of $[Mn^V(O)(TBP_8Cz)(N_3)]^-$ (634 nm) (open blue square) together with best fits (solid black line).

mechanism shown in Scheme 2. The resulting fits yielded pseudo-first-order rate constants (k_{obs}), which were found to be linearly dependent on substrate concentration (Figure 5). The best-fit lines of k_{obs} versus [substrate] yielded second-order rate constants (k) (Table 1) for the different axial donors.

As can be seen from Table 1, there is a remarkable enhancement in OAT reactivity for the $Mn^V(O)$ complex in the presence of anionic donors. The second-order rate constant for F^- reveals a dramatic rate enhancement of 1100-fold in the oxidation of DMS compared to the five-coordinate $Mn^V(O)$ complex. A similar rate enhancement (1700) is seen for the oxidation of DBS. Addition of CN^- as the axial donor has an even more dramatic effect, revealing a rate enhancement of 24,000 for DBS oxidation by the $[Mn^V(O)(TBP_8Cz)(CN)]^-$ complex.

Further examination of the other anionic axial donors in Table 1 reveals some important trends. The addition of azide (N_3^-) leads to a 70-fold rate enhancement over the five-coordinate complex in the sulfoxidation of DMS. The cyanate (OCN^-) anion gives a more modest increase of only 1.5 times for reaction with DMS, and the nitrate (NO_3^-) anion showed essentially no influence. The thiocyanate (SCN^-) anion also has little effect over the reaction rate with DBS as substrate. Taken together, the kinetic data indicate the following trend regarding the influence of the anionic donors on the rate of OAT: none $\approx SCN^- \approx NO_3^- < OCN^- < N_3^- < F^- \ll CN^-$. This trend is supported by our DFT calculations and suggests a possible structural explanation for the relative influence of X^- on the reactivity of $Mn^V(O)$-(TBP_8Cz) (vide infra).

Influence of *para*-Substituents on the Reactivity of Thioanisole Derivatives. The reactive cyanide-ligated $[Mn^V(O)(TBP_8Cz)(CN)]^-$ complex was chosen for further study with a series of p-X-$C_6H_4SCH_3$ derivatives (Scheme 3). The oxidation of $C_6H_5SCH_3$ proceeds in good yield (84%) to give the mono-oxygenated sulfoxide product, with 71% of the ^{18}O label in $[Mn^V(^{18}O)(TBP_8Cz)(CN)]^-$ transferring to the sulfur atom.[36] The reactions between the p-X-substituted thioanisole derivatives and $[Mn^V(O)(TBP_8Cz)(CN)]^-$ were monitored by UV−vis spectroscopy, and good isosbestic behavior for the conversion of the Mn^V starting material to the
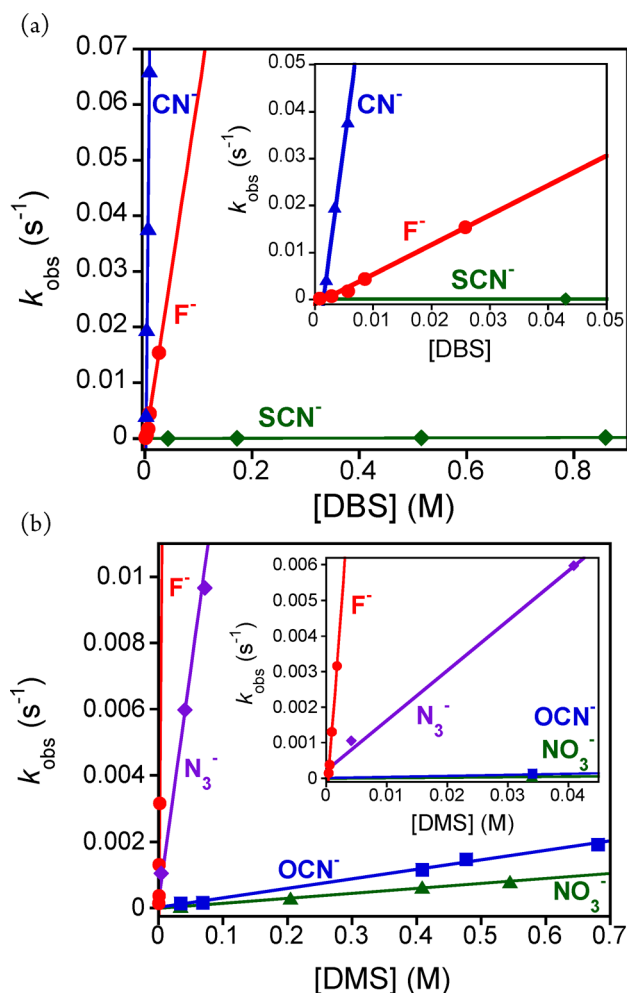

Figure 5. (a) Plots of k_{obs} versus concentration of DBS for $X^- = CN^-$ (solid blue triangle), F^- (solid red circle), and SCN^- (solid green diamond). Inset: expanded region from 0 to 0.05 M. (b) Plots of k_{obs} versus concentration of DMS for $X^- = F^-$ (solid red circle), N_3^- (solid purple diamond), OCN^- (solid blue square) and NO_3^- (solid green triangle). Inset: expanded region from 0 to 0.045 M.

Table 1. Second-Order Rate Constants for OAT to Thioether Substrates

axial ligand	substrate	k (M^{-1} s^{-1})	$k[Mn^V(O)(X)]^-/k[Mn^V(O)]$
none[a,b]	DBS	3.8×10^{-4}	
CN[a,c]	DBS	9.2 ± 0.3	24,000
F	DBS	0.63 ± 0.02	1700
SCN	DBS	$(1.5 \pm 0.1) \times 10^{-4}$	0.4
none[b]	DMS	$(2.0 \pm 0.2) \times 10^{-3}$	
F	DMS	2.3 ± 0.3	1100
N_3	DMS	0.14 ± 0.01	70
OCN	DMS	$(2.9 \pm 0.3) \times 10^{-3}$	1.5
NO_3	DMS	$(1.5 \pm 0.1) \times 10^{-3}$	0.75

[a]In toluene. [b]Ref 40. [c]Ref 36.

$[Mn^{III}(CN)]^-$ product was seen for all substrates. The resulting pseudo-first-order rate constants (k_X) for the different *para*-substituted derivatives were used to construct the Hammett plot shown in Figure 6. For the electron-donating substituents, there is a good linear correlation with a clear negative slope of rho (ρ) = −1.29. This trend is easily explained by a mechanism involving electrophilic attack of the oxo group of the $Mn^V(O)$ complex on

Scheme 3. OAT to *para*-Substituted Thioanisole Derivatives

X = -OMe, -CH$_3$, -H, -Br, -COOMe, -CN, -NO$_2$
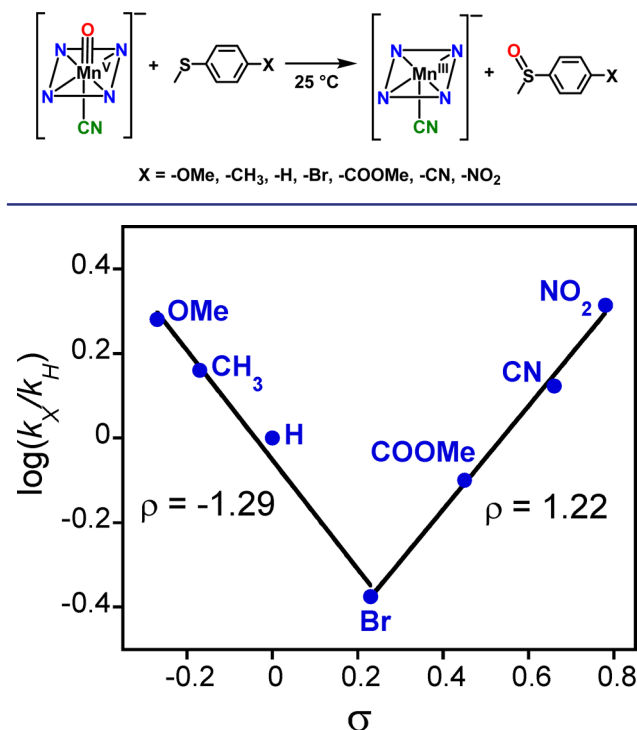
Figure 6. Hammett plot for the reaction of $[Mn^V(O)(TBP_8Cz)(CN)]^-$ and *para*-X-substituted thioanisole derivatives.

the sulfur center of the thioanisole derivatives. A negative ρ value was also seen for H-atom abstraction by the five-coordinate $Mn^V(O)$ complex with a series of *p*-substituted phenols.[45] These data indicate that the anionic, six-coordinate $Mn^V(O)$ complex maintains significant electrophilic character. However, the electron-withdrawing *p*-COOMe, *p*-CN, and *p*-NO$_2$ substituents lead to a substantial *increase* in reaction rate and a *positive* rho value of $\rho = +1.22$. Such a "V-shaped" Hammett plot suggests a distinct change in mechanism for the electron-poor substrates. For comparison, a V-shaped Hammett plot was observed for a related $Mn^V(imido)(corrole)$ complex, also implicating a mechanistic switch.[46] The generality of this change in mechanism for the six-coordinate anionic $Mn^V(O)$ complexes was confirmed by examining the fluoride-ligated $[Mn^V(O)-(TBP_8Cz)(F)]^-$. Reaction of this complex with *p*-X-C$_6$H$_4$SCH$_3$ derivatives also revealed a clear V-shaped Hammett plot (Figure S14).

A possible explanation for the V-shaped Hammett plots comes from consideration of the contributing resonance structures shown in Figure 7. The quinoid-type resonance forms may be partly stabilized by the electron-withdrawing *p*-COOMe, *p*-CN,
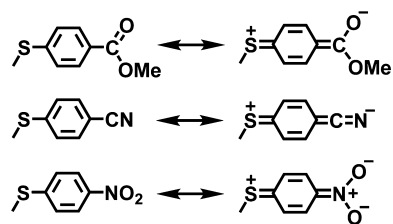
Figure 7. Resonance structures for electron-withdrawing *para*-subsituted thioanisole derivatives.

and *p*-NO$_2$ substituents. Evidence for the contribution of a similar quinoid-type resonance form in a *p*-nitrophenylthiolate–Ni^{II} complex was observed by X-ray crystallography.[47] The quinoid-type resonance form shown in Figure 7 generates partial positive charge on the sulfur center, making these relatively electron-poor substrates potentially *electrophilic* in nature. A different mechanism for sulfoxidation could then result for the *p*-COOMe, *p*-CN, and *p*-NO$_2$ substrates.

The two possible mechanistic scenarios are shown in Scheme 4. Pathway A corresponds to the electron-donating *para*-X

Scheme 4. Possible Mechanistic Pathways for Electron-Donating (Pathway A) and Electron-Withdrawing (Pathway B) *para*-Substituted Thioanisole Derivatives
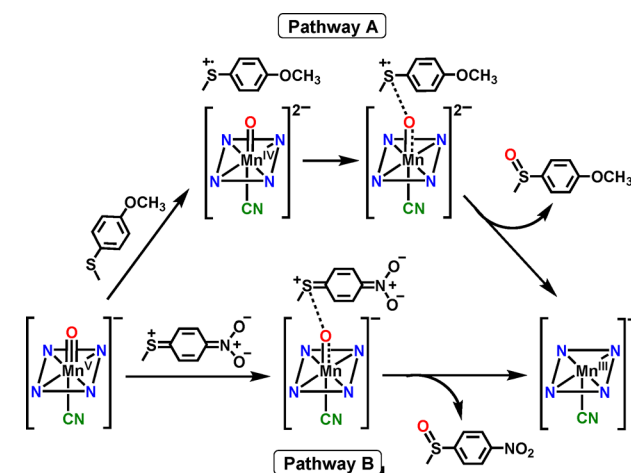
substituents and shows the sulfoxidation reaction formally broken into electron-transfer and O–S bond formation steps. The redox potentials of the thioether substrates ($E°_{ox} = 1.2–1.6$ V vs SCE) as compared to the parent five-coordinate $Mn^V(O)$ complex ($E_{1/2} = -0.05$ V vs SCE)[37] indicate that pure outer-sphere ET between ArSR and the six-coordinate, anionic $Mn^V(O)$ complexes is likely to be thermodynamically highly disfavored. Thus, a more reasonable mechanism, which we favor, involves a single transition state with contributions from both the ET and S–O bond formation steps formally depicted in Pathway A. The rates for the electron-donating substituents correlate with the trend expected from a significant contribution of the ET process, which should get slower as the redox potential of the thioether increases. In contrast, the electron-withdrawing substituents may exhibit negligible contribution from electron-transfer because of their very high redox potentials. For these substrates, the quinoid-type resonance structure can enhance the rate of S–O bond formation, taking advantage of the ability of the anionic $[Mn^V(O)(TBP_8Cz)(X)]^-$ (X = CN$^-$ or F$^-$) complex to serve as a potential weak nucleophile.[48,49] Thus, for pathway B, the transition state is dominated by S–O bond formation. This barrier would be lower for more electron-withdrawing substrates, providing an explanation for the positive ρ value and the V-shaped Hammett plot seen in Figure 6.

The *cationic* complex $Mn^V(O)(TBP_8Cz^{\bullet+})$ was previously prepared by some of us and, to our knowledge, is the only example of an $Mn^V(O)(\pi$-radical cation) complex. This *cationic* complex functioned as an electrophilic oxidant toward phosphine and thioether substrates and was an ideal candidate for comparison of its OAT reactivity with the *anionic* axially ligated $Mn^V(O)$ complexes. The $Mn^V(O)(\pi$-radical cation) complex

13850

dx.doi.org/10.1021/ja507177h | *J. Am. Chem. Soc.* 2014, 136, 13845–13852

was generated by chemical oxidation of the neutral $Mn^V(O)$ starting material with the one-electron oxidant $[(4-BrC_6H_4)_3N^{\bullet+}](SbCl_6^-)$ (Scheme 5). Isosbestic behavior was

Scheme 5. Generation and OAT Reaction of the Cationic $[Mn^V(O)(TBP_8Cz^{+\bullet})]$ Complex
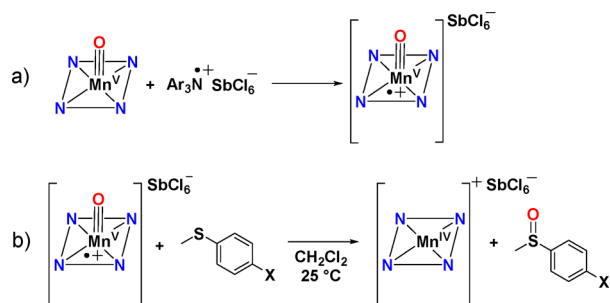
observed for the reactions with the *p*-X-substituted thioanisole derivatives, and in this case the two-electron reduced product of $Mn^V(O)(TBP_8Cz^{\bullet+})$ is the Mn^{IV} complex $[Mn^{IV}(TBP_8Cz)]^+$, as expected following OAT. The resulting Hammett plot of $\log(k_X/k_H)$ versus σ values for the *para*-X derivatives is shown in Figure 8. A strong linear correlation with a slope $\rho = -1.40$ is found
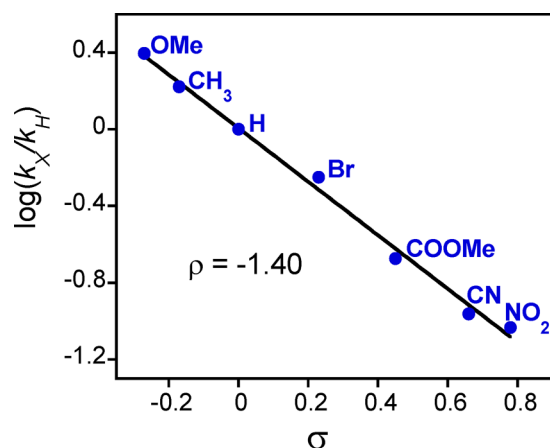
Figure 8. Hammett plot for the reaction of $Mn^V(O)(TBP_8Cz^{+\bullet})$ with *para*-X-substituted thioanisole derivatives in CH_2Cl_2.

throughout the range of *para*-X derivatives, in stark contrast to the V-shaped Hammett plot seen for the anionic $[Mn^V(O)-(TBP_8Cz)(X)]^-$ ($X = CN^-$ or F^-). A single mechanism involving electrophilic attack of $Mn^V(O)(TBP_8Cz^{\bullet+})$ (Pathway A) is inferred. These findings provide strong support for the conclusion that there is a mechanistic switch for the CN^- and F^- complexes and the electron-poor substrates (Pathway B), and it is the *anionic* nature of the CN^- and F^- species that likely facilitates the opening of this unique reaction channel.

Density Functional Theory (DFT) Calculations. Computational studies were undertaken to help explain the trend in reactivity for the different anionic axial ligands. Calculations were performed at RIJCOSX-B3LYP/LANLDZ/6-31G level of theory, and the optimized geometries revealed a variation in Mn^V–X bond distances that were used for a qualitative comparison of the binding interactions for the various axial (X^-) donors. The TBP groups were replaced with H-atoms on the Cz ligand to facilitate the computations. The calculations were performed on the singlet state only for the Mn^V ion, which

has been shown to be the ground state in previous calculations[35,40] and which is consistent with XAS measurements for the CN^- complex.[36] The optimized geometries for the six-coordinate F^- and CN^- structures were calculated previously[35] but were repeated here for comparative purposes. The calculated structures for $^1[Mn^V(O)(H_8Cz)(X)]^-$ ($X = F^-$, CN^-) revealed Mn–X distances (Table 2) indicating a binding interaction. The

Table 2. Select Bond Distances (Å) from DFT Calculations

	none	CN^-	F^-	N_3^-	OCN^-	NO_3^-
Mn^V–O	1.549	1.568	1.568	1.568	1.561	1.557
Mn^V–X	–	2.146	1.931	2.354	2.420	2.518

azide and cyanate anions also remained bound to the metal following optimization but exhibit longer bond distances. Interestingly, the nitrate anion binds only very weakly, and thiocyanate (not shown in Table 2) dissociates completely from the metal upon geometry optimization. Both NO_3^- and SCN^- anions showed no influence on the rate of OAT. The computational results show that the Mn^V–X distance correlates well with the trend in reactivity for the axial donors, in which the shorter distances seen for CN^- and F^- correspond to large rate enhancements, whereas the other ligands exhibit either weak or no influence on OAT rates.

■ CONCLUSIONS

Addition of anionic axial donors (X^-) to an $Mn^V(O)$ corrolazine results in binding to the Mn^V center. Resonance Raman spectroscopy confirms a subtle weakening of the Mn^V–O triple bond upon addition of the X^- ligand, providing strong evidence for coordination of X^- in a position *trans* to the terminal oxo group. The axial donors CN^- and F^- lead to dramatic increases in OAT reactivity to thioether substrates, and N_3^- also shows a strong effect. The OCN^-, NO_3^-, and SCN^- anions, however, exhibit little or no influence on OAT. These trends in reactivity correlate well with the trend in the DFT-derived Mn^V–X distances. A Hammett analysis with a range of *p*-X-$C_6H_4SCH_3$ derivatives revealed an unusual V-shaped Hammett plot for $[Mn^V(O)(TBP_8Cz)(X)]^-$ ($X = CN^-$ or F^-) complexes, indicating a distinct change in mechanism for OAT to the thioether substrates. This Hammett behavior strongly contrasts the linear plot seen for the cationic complex $Mn^V(O)-(TBP_8Cz^{\bullet+})$. These findings suggest a novel bifurcated mechanistic scenario in which the axially ligated anionic complexes can function in either a purely electrophilic capacity or in an initial nucleophilic manner when strong electron-withdrawing substituents are present on the thioanisole derivatives. Our results suggest that axial ligation is a key factor in the OAT reactivity of $Mn^V(O)$ complexes, and the addition of the appropriate axial donor can be a good strategy for dramatically increasing OAT reactivity. Even though the axially ligated complexes bear an overall negative charge, they function as more powerful, electrophilic oxidizing agents as compared to the nonligated, neutral $Mn^V(O)$ precursor complex. With the strong electron-withdrawing *p*-X substituents on the thioanisole derivatives, the nucleophilic properties of the anionic $Mn^V(O)$ complexes provide a further boost to their reactivity. These new mechanistic insights should help in our understanding of axial ligand effects in heme enzymes as well as in the potential design of new synthetic oxidation catalysts.

■ AUTHOR INFORMATION

Corresponding Authors

dpg@jhu.edu
mtg10@psu.edu
sam.devisser@manchester.ac.uk

Notes

The authors declare no competing financial interest.

■ REFERENCES

(1) Green, M. T. *Curr. Opin. Chem. Biol.* **2009**, *13*, 84−88.

(2) Groves, J. T. *Nat. Chem.* **2014**, *6*, 89−91.

(3) Denisov, I. G.; Makris, T. M.; Sligar, S. G.; Schlichting, I. *Chem. Rev.* **2005**, *105*, 2253−2277.

(4) Rittle, J.; Green, M. T. *Science* **2010**, *330*, 933−937.

(5) Yosca, T. H.; Rittle, J.; Krest, C. M.; Onderko, E. L.; Silakov, A.; Calixto, J. C.; Behan, R. K.; Green, M. T. *Science* **2013**, *342*, 825−829.

(6) Poulos, T. L.; Finzel, B. C.; Howard, A. J. *J. Mol. Biol.* **1987**, *195*, 687−700.

(7) de Visser, S. P.; Shaik, S.; Sharma, P. K.; Kumar, D.; Thiel, W. *J. Am. Chem. Soc.* **2003**, *125*, 15779−15788.

(8) Poulos, T. L. In *Handbook of Porphyrin Science*; Kadish, K. M., Smith, K. M.; Guilard, R., Eds.; World Scientific Publishing Co.: Singapore, 2012; Vol. 19, p 45−109.

(9) Battistuzzi, G.; Bellei, M.; Bortolotti, C. A.; Sola, M. *Arch. Biochem. Biophys.* **2010**, *500*, 21−36.

(10) Bewley, K. D.; Ellis, K. E.; Firer-Sherwood, M. A.; Elliott, S. J. *Biochim. Biophys. Acta, Bioenerg.* **2013**, *1827*, 938−948.

(11) Diaz, A.; Loewen, P. C.; Fita, I.; Carpena, X. *Arch. Biochem. Biophys.* **2012**, *525*, 102−110.

(12) Alfonso-Prieto, M.; Vidossich, P.; Rovira, C. *Arch. Biochem. Biophys.* **2012**, *525*, 121−130.

(13) Gross, Z. *J. Biol. Inorg. Chem.* **1996**, *1*, 368−371.

(14) Kang, Y.; Chen, H.; Jeong, Y. J.; Lai, W.; Bae, E. H.; Shaik, S.; Nam, W. *Chem.—Eur. J.* **2009**, *15*, 10039−10046.

(15) Takahashi, A.; Yamaki, D.; Ikemura, K.; Kurahashi, T.; Ogura, T.; Hada, M.; Fujii, H. *Inorg. Chem.* **2012**, *51*, 7296−7305.

(16) Takahashi, A.; Kurahashi, T.; Fujii, H. *Inorg. Chem.* **2009**, *48*, 2614−2625.

(17) Song, W. J.; Ryu, Y. O.; Song, R.; Nam, W. *J. Biol. Inorg. Chem.* **2005**, *10*, 294−304.

(18) Pan, Z. Z.; Zhang, R.; Newcomb, M. *J. Inorg. Biochem.* **2006**, *100*, 524−532.

(19) Hessenauer-Ilicheva, N.; Franke, A.; Meyer, D.; Woggon, W. D.; van Eldik, R. *J. Am. Chem. Soc.* **2007**, *129*, 12473−12479.

(20) Kumar, D.; Karamzadeh, B.; Sastry, G. N.; de Visser, S. P. *J. Am. Chem. Soc.* **2010**, *132*, 7656−7667.

(21) Ohno, T.; Suzuki, N.; Dokoh, T.; Urano, Y.; Kikuchi, K.; Hirobe, M.; Higuchi, T.; Nagano, T. *J. Inorg. Biochem.* **2000**, *82*, 123−125.

(22) Kumar, A.; Goldberg, I.; Botoshansky, M.; Buchman, Y.; Gross, Z. *J. Am. Chem. Soc.* **2010**, *132*, 15233−15245.

(23) Liu, H. Y.; Zhou, H.; Liu, L. Y.; Ying, X.; Jiang, H. F.; Chang, C. K. *Chem. Lett.* **2007**, *36*, 274−275.

(24) Solati, Z.; Hashemi, M.; Hashemnia, S.; Shahsevani, E.; Karmand, Z. *J. Mol. Catal. A: Chem.* **2013**, *374*, 27−31.

(25) Jin, N.; Ibrahim, M.; Spiro, T. G.; Groves, J. T. *J. Am. Chem. Soc.* **2007**, *129*, 12416−12417.

(26) Arunkumar, C.; Lee, Y. M.; Lee, J. Y.; Fukuzumi, S.; Nam, W. *Chem.—Eur. J.* **2009**, *15*, 11482−11489.

(27) Song, W. J.; Seo, M. S.; George, S. D.; Ohta, T.; Song, R.; Kang, M. J.; Tosha, T.; Kitagawa, T.; Solomon, E. I.; Nam, W. *J. Am. Chem. Soc.* **2007**, *129*, 1268−1277.

(28) Latifi, R.; Tahsini, L.; Karamzadeh, B.; Safari, N.; Nam, W.; de Visser, S. P. *Arch. Biochem. Biophys.* **2011**, *507*, 4−13.

(29) Park, S. E.; Song, W. J.; Ryu, Y. O.; Lim, M. H.; Song, R.; Kim, K. M.; Nam, W. *J. Inorg. Biochem.* **2005**, *99*, 424−431.

(30) Jin, N.; Lahaye, D. E.; Groves, J. T. *Inorg. Chem.* **2010**, *49*, 11516−11524.

(31) Wang, C.; Kurahashi, T.; Inomata, K.; Hada, M.; Fujii, H. *Inorg. Chem.* **2013**, *52*, 9557−9566.

(32) Kurahashi, T.; Kikuchi, A.; Shiro, Y.; Hada, M.; Fujii, H. *Inorg. Chem.* **2010**, *49*, 6664−6672.

(33) Kurahashi, T.; Fujii, H. *Bull. Chem. Soc. Jpn.* **2012**, *85*, 940−947.

(34) Collman, J. P.; Zeng, L.; Brauman, J. I. *Inorg. Chem.* **2004**, *43*, 2672−2679.

(35) Prokop, K. A.; de Visser, S. P.; Goldberg, D. P. *Angew. Chem., Int. Ed.* **2010**, *49*, 5091−5095.

(36) Neu, H. M.; Quesne, M. G.; Yang, T.; Prokop-Prigge, K. A.; Lancaster, K. M.; Donohoe, J.; DeBeer, S.; de Visser, S. P.; Goldberg, D. P. *Chem. Eur. J.*, accepted; DOI: 10.1002/chem.201404349.

(37) Lansky, D. E.; Mandimutsira, B.; Ramdhanie, B.; Clausen, M.; Penner-Hahn, J.; Zvyagin, S. A.; Telser, J.; Krzystek, J.; Zhan, R.; Ou, Z.; Kadish, K. M.; Zakharov, L.; Rheingold, A. L.; Goldberg, D. P. *Inorg. Chem.* **2005**, *44*, 4485−4498.

(38) Wright, M. R. *An Introduction to Chemical Kinetics*; Wiley: Chichester, U.K., 2004.

(39) Hansch, C.; Leo, A.; Taft, R. W. *Chem. Rev.* **1991**, *91*, 165−195.

(40) Prokop, K. A.; Neu, H. M.; de Visser, S. P.; Goldberg, D. P. *J. Am. Chem. Soc.* **2011**, *133*, 15874−15877.

(41) Lansky, D. E.; Narducci Sarjeant, A. A.; Goldberg, D. P. *Angew. Chem., Int. Ed.* **2006**, *45*, 8214−8217.

(42) Mandimutsira, B. S.; Ramdhanie, B.; Todd, R. C.; Wang, H.; Zareba, A. A.; Czernuszewicz, R. S.; Goldberg, D. P. *J. Am. Chem. Soc.* **2002**, *124*, 15170−15171.

(43) Jackson, T. A.; Rohde, J. U.; Seo, M. S.; Sastri, C. V.; DeHont, R.; Stubna, A.; Ohta, T.; Kitagawa, T.; Münck, E.; Nam, W.; Que, L., Jr. *J. Am. Chem. Soc.* **2008**, *130*, 12394−12407.

(44) Czarnecki, K.; Nimri, S.; Gross, Z.; Proniewicz, L. M.; Kincaid, J. R. *J. Am. Chem. Soc.* **1996**, *118*, 2929−2935.

(45) Lansky, D. E.; Goldberg, D. P. *Inorg. Chem.* **2006**, *45*, 5119−5125.

(46) Zdilla, M. J.; Dexheimer, J. L.; Abu-Omar, M. M. *J. Am. Chem. Soc.* **2007**, *129*, 11505−11511.

(47) Nakazawa, J.; Ogiwara, H.; Kashiwazaki, Y.; Ishii, A.; Imamura, N.; Samejima, Y.; Hikichi, S. *Inorg. Chem.* **2011**, *50*, 9933−9935.

(48) Leeladee, P.; Baglia, R. A.; Prokop, K. A.; Latifi, R.; de Visser, S. P.; Goldberg, D. P. *J. Am. Chem. Soc.* **2012**, *134*, 10397−10400.

(49) Smeltz, J. L.; Lilly, C. P.; Boyle, P. D.; Ison, E. A. *J. Am. Chem. Soc.* **2013**, *135*, 9433−9441.